Current Research in Green and Sustainable Chemistry 6 (2023) 100363

Contents lists available at ScienceDirect

Current Research in Green and Sustainable Chemistry

journal homepage: www.elsevier.com/journals/current-research-in-green-and-sustainable-chemistry/2666-0865

Correlation between morphology and performance of cellulose nanofibril-based films

Liqing Wei [a,b], Huiyang Bian [c,d], Umesh P. Agarwal [a], Ronald C. Sabo [a], Laurent M. Matuana [e], Nicole M. Stark [a,e,*]

[a] USDA Forest Service, Forest Products Laboratory, Madison, WI, 53705, USA
[b] Hanwha Azdel, Inc., 2000 Enterprise Drive, Forest, VA, 24551, USA
[c] Jiangsu Co-Innovation Center of Efficient Processing and Utilization of Forest Resources, Nanjing Forestry University, Nanjing, 210037, China
[d] International Innovation Center for Forest Chemicals and Materials, Nanjing Forestry University, Nanjing, 210037, China
[e] Michigan State University, School of Packaging, East Lansing, MI, 48824, USA

ARTICLE INFO

Keywords:
Cellulose nanofibrils
Microfluidization
Water vapor permeability
Oxygen permeability
Transparency
Surface roughness
Morphology

ABSTRACT

Cellulose nanofibrils (CNFs) were produced from bleached eucalyptus kraft pulp using microfluidization varying the number of passes through the microfluidizer. CNFs were processed into dry films to elucidate the effect of CNFs morphology on the physical, optical and barrier properties of the films. As the number of passes through the microfluidizer increased, the fibril diameter and degree of polymerization decreased. A higher number of passes produced CNFs with smaller diameter resulting in CNF films with smaller root mean surface (RMS) roughness, higher tensile strength and Young's modulus, and higher transparency. CNF films with lower porosity had lower water vapor permeability (WVP) at 50% RH (better barrier properties), but the number of passes did not significantly affect water vapor permeability at 90% RH or oxygen permeability at 50% RH or 90% RH. Increasing the number of microfluidization passes resulted in CNF films with higher density, lower crystallinity, and higher water accessibility. The results suggest that the physical properties, such as density, of the film were more dominant for the mechanism of WVP compared with crystallinity and water accessibility. A model of water vapor transmission through the CNF film was proposed. By establishing a relationship between CNFs morphology and performance characteristics of corresponding films, especially for barrier properties, insights were obtained that would be beneficial for food packaging applications.

1. Introduction

It has become increasingly desirable to develop sustainable packaging with high performance. Cellulose nanomaterials [cellulose nanocrystals (CNCs) and cellulose nanofibrils (CNFs)], derived from the most abundant biopolymer on earth, cellulose, have become attractive as a material for sustainable packaging applications because of their good biodegradability, biocompatibility, and renewability [1,2]. In addition, CNF films have drawn much more attention in food packaging because they have low toxicity, adequate mechanical properties and provide sufficient barriers to oxygen, grease, and other contaminants in order to obtain a satisfactory shelf life and to prevent food deterioration [1–5]. Numerous studies have found that cellulose nanomaterial films and coatings have the potential for barrier, but more work is needed to understand the dominating characteristics of the nanomaterials that lead to good barriers.

Mechanical fibrillation is a common approach for CNFs production but may be energy-consuming [6–10]. A multistep pretreatment, e.g., chemical and enzymatic treatments, can reduce energy consumption for producing CNFs, but issues such as low yield and high cost for chemical recovery/recycling need to be addressed for commercial application [11,12]. In recent years, disk milling as with a supermasscolloider (SMC) has gained much attention for its feasibility of commercial scale-up [13]. Mechanical fibrillation by disk milling causes a series of dramatic changes in fiber pulps, such as internal fibrillation, external fibrillation and fiber shortening. Typical operation conditions are 1.0–2.0 wt% solids loading and disk rotating speed at 1500 rpm which is higher than that used in microfluidization or homogenization processes [14]. However, the fibril diameter of CNFs is less homogenous compared with CNFs produced using high-pressure homogenization or

* Corresponding author. USDA Forest Service, Forest Products Laboratory, Madison, WI, 53705, USA.
E-mail address: nicole.stark@usda.gov (N.M. Stark).

https://doi.org/10.1016/j.crgsc.2023.100363
Received 7 February 2023; Received in revised form 2 May 2023; Accepted 18 May 2023
Available online 19 May 2023

microfluidization, with large bundles of fibrils clearly observed [12,15]. Thus, further nanofibrillation must be applied to produce more homogenous CNFs.

Information on CNF morphology, degree of polymerization (DP) and crystalline structure of CNFs would be useful to determine the performance characteristics of CNF films. Film characteristics such as mechanical properties, transparency, water accessibility, and barrier properties are important for food packaging. However, there is limited information available on the relationship between CNF film structure and performance. Recently developed Raman spectroscopy methods have been used to quantitatively evaluate the crystalline structure and water accessibility of cellulose nanomaterials [16]. Nevertheless, the relationship between water accessibility (or crystalline structure) and water vapor transmission properties for CNF film has not been reported. For example, does the mechanism of water vapor permeation through CNF film depend upon the physical structure of the film (i.e., density or compact structure of CNFs), or water accessibility and crystalline structure of CNF film?

In the present study, we aim to both further understand the effect of processing on properties of CNFs and to further develop characterization techniques, such as water accessibility measurements, for evaluation of films and papers produced from cellulose nanomaterials. Here, pure mechanical fibrillation using disk milling followed by post-treatment, i.e., microfluidization, was applied to produce homogeneous CNFs. Properties of the CNF films, made from suspensions passing through the microfluidizer for a different number of times (0, 15, 30 and 50 times), were compared and evaluated for degree of polymerization, surface morphology, mechanical properties, optical/transparency, barrier properties, crystallinity and water accessibility. Measurement of water accessibility is facile and may provide valuable information about the structure and performance of cellulose-based packaging materials.

2. Materials and methods

2.1. Materials

Bleached eucalyptus kraft pulp (BEP, Aracruz Cellulose, Brazil) was purchased in dry form and used as the raw material. This is the material typically used for the production of CNFs produced at FPL at the pilot scale [17]. After soaking in distilled water for at least 24 h, the pulp was disintegrated by shear mixing in a blender for 10 min. The mixture of pulp fiber and water was centrifuged and concentrated to 2 wt% consistency, which was employed for subsequent mechanical disintegrations.

2.2. Cellulose nanofibril production

The pulp fibers were mechanically fibrillated at initial solids loading of 2 wt% using a MKZA6-2 Super Mass Colloider (Masuko Sangyo Co. Ltd, Saitama, Japan) at 1500 rpm as described previously [18]. The SMC is equipped with two stone grinding disks (Disk Model: MKGA6-80#) and positioned on top of each other. The bottom disk rotates while the top disk is stationary. Pulp fiber suspension was fed into the disk grinder continuously by gravity using a loop consisting of a peristaltic pump (Cole Parmer, Chicago, IL) and plastic tubing. The gap of the two disks was adjusted to −200 μm from motion zero position after pulp fibers were loaded. The motion zero position was determined right at the contact position between the two grinding disks before loading pulp fibers. Due to the presence of pulp fibers, there was no direct contact between the two grinding stones even at a negative setting of disk position. Approximately 500 g pulp fibers (on a dry basis) were ground for 8 h and stored in plastic bags.

A portion of the pulp refined for 8 h in the SMC was further fibrillated using a microfluidizer (M-110EH, Microfluidics Corp., Westwood, MA). The refined pulp fiber slurry was diluted to 1 wt% solids consistency and passed through the 200 μm chamber up to 10 passes, and then passed through an 87 μm chamber for with operation pressure of 150 MPa for a varying number of passes (15, 30, or 50). All cellulose nanofibril suspensions were stored at 4 °C for further characterization and processing into films. The sample refined in the SMC but not microfluidized was denoted as P0, while fibrils obtained after passing through the 87 μm chamber for 15, 30, and 50 times were coded as P15, P30, and P50, respectively.

2.3. Preparation of CNF films

The CNF films were prepared by filtering CNF suspensions, followed by air drying. The nanofibril solutions were diluted to the concentration of 0.2 wt%, followed by mechanical stirring for 30 min, and then filtered using a 142 mm diameter Millipore ultrafiltration system (Millipore, Millipore Corporation, USA) under 0.55 MPa air pressure. Omnipore TM filter membranes with a pore size of 0.1 μm (JVWP14225, JV, Millipore Corporation, USA) were used in the apparatus with support of a plain filter paper (slow flow rate, Fisherbrand, USA). After water was filtered out, the film was left on the apparatus for another 2 h before air was released. The wet films were peeled from the membrane and stacked first between waxy coated papers and blotting papers. This assembly was maintained in between two metal plates and was air dried at room temperature for two weeks under a load of 23 kg. The films were then conditioned at 50% relative humidity (RH) and 23 °C until tested.

2.4. Degree of polymerization

The degree of polymerization (*DP*) for fibrils was estimated based on the intrinsic viscosity following the method reported previously [19]. Vacuum dried cellulosic solids of 0.1 g was first dispersed in 10 mL DI water, then added 10 mL of 1 M cupriethylenediamine solution. The viscosity of the resultant solution was measured in a capillary viscometer at 25 °C. The *DP* value was then calculated by the following Eq. (1):

$$DP^{0.905} = \frac{[\eta]}{c} \times k \tag{1}$$

where [η] is the intrinsic viscosity of cellulosic solution (g/mL); c is the concentration of solution (g/mL); and k is an empirical constant of 0.75. Duplicate measurements were conducted and the averages were reported.

2.5. Morphology

The morphologies of CNFs and resulting films were observed using atomic force microscopy (CS-3230, AFM workshop, Signal Hill, CA, USA). Suspensions of approximately 0.01 wt% CNF were deposited onto clean mica substrates and air dried overnight at room temperature. CNF films were also fixed on the mica substrates. Images were taken in vibrating mode (160–225 kHz) with a radius of the tip curvature of 10–15 nm. Fibril heights were measured using Gwyddion (Department of Nanometrology, Czech Metrology Institute, Crezh Republic, 64-bit). The root mean square (RMS) roughness was reported for AFM images of the CNF films.

2.6. Density and porosity

The density of CNF film was estimated gravimetrically based on the weight and volume of a square specimen ($10 \times 10 \times 0.07$ mm^3) cut with a homemade stainless-steel die. The porosity was estimated as the following Eq. (2):

$$\text{Porosity } (\%) = \left(1 - \frac{\rho_{\text{film}}}{\rho_{\text{cellulose}}}\right) \times 100 \tag{2}$$

where ρ_{film} and $\rho_{\text{cellulose}}$ represent the density of the obtained CNF films and neat cellulose (1.5 g/cm^3), respectively.

2.7. Tensile testing

The tensile properties of different CNF films were tested using the T5002 MTS testing machine with a 500 N load cell, according to ASTM D638. The specimens were cut to conform to ASTM D638 type V dog-bone shape using a die (Qualitest, FL, USA). Samples were conditioned at 50% RH and 23 °C for one week prior to test. The specimens were pre-loaded with 5 N of force to remove slack, and the tests were performed with a crosshead speed of 1 mm/min. Ten measurements were carried out for each CNF film and the averages and standard errors were reported. Significant differences between values were determined using Student's t-test. It was assumed the two groups being compared had unequal variance, the hypothesis was two-tailed, and significance was determined at $\alpha = 0.05$.

2.8. UV–vis spectroscopic analysis

The visible light transmittance of CNF films was recorded using a UV–vis spectrophotometer (model 8453 Agilent, Palo Alto, CA). The instrument is equipped with a kinetic operation mode for continuously recording complete spectra in a frequency of every 10 s. The transmittance was normalized to a similar thickness, i.e., 10 μm, between duplicates, according to Beer-Lambert Law as shown in Eq. (3):

$$\varepsilon = \frac{C \times \log T}{d} \tag{3}$$

where ε is the molar absorptivity, T is the transmittance value, C is sample concentration in moles/L, and d is the specimen thickness in cm.

2.9. Barrier properties

Water vapor permeability of the CNF films was determined gravimetrically, following the desiccant method in ASTM E96 with 68–3000 EZ-Cup vapometer assemblies (Thwing-Albert Instrument Company, West Berlin, NJ, USA). The diameter of the cup openings measured 6.35 cm. Desiccant (anhydrous calcium chloride) was placed in the base of the cup within 6 mm of the specimen. The specimen was placed onto the cup and held in place with an aluminum threaded flanged ring with two neoprene gaskets with a Teflon seal. Each assembly was weighed and placed in two rooms under controlled conditions: (i) 21.1 °C with 50% RH; (ii) 26.7 °C with 90% RH. The samples were weighed periodically to establish the linear region for the curve of weight gain (G) as a function of time (t). Water vapor transmission rate (WVTR) was calculated based on Eq. (4):

$$\mathrm{WVTR} = \frac{G}{t} \times A \tag{4}$$

where G/t is the slope of the fitted straight line and A is the area of the film exposed to air, which was equal to 3167 mm^2.

The film water vapor permeability (WVP) was calculated by Eq. (5):

$$\mathrm{WVP} = \frac{\mathrm{WVTR}}{\Delta_\rho} \times d = \frac{\mathrm{WVTR}}{(R_1 - R_2) \times S} \times d \tag{5}$$

where Δ_ρ is the vapor pressure difference, S is the saturation vapor pressure of water at the test temperature ($S_{21.1°C} = 2493$ Pa or $S_{26.7°C} = 3493$ Pa), R_1 is the fractional RH on the vapor source side (50% or 90%) and R_2 is the fractional RH on the sink side (0%), and d is the thickness of the sample. Three samples of each formulation were tested.

Oxygen transmission rate (OTR), the volume of oxygen through the film per unit surface area, was determined using a fully automated oxygen transmission rate test system (MOCON OX-TRAN 2/22 L, Minneapolis, MN) following standard ASTM D3985. The sample thickness was recorded in 5 locations before mounting in holders with an exposure area of 50 cm^2. An individual zero was collected at the beginning of the test, followed by 36 exposure cycles, each 60 min long. An instrument rezero ran after every two tests for 30 min. The cell temperature was 23 °C. Samples were exposed to three different relative humidities (0%, 50%, and 90%) run sequentially. Two replicates were run for each series of tests. The oxygen permeability (OP) was calculated as the OTR divided by the partial pressure of oxygen (the mole fraction of oxygen multiplied by 1 atm) and multiplied by film thickness (d).

$$\mathrm{OP} = \frac{OTR}{\rho} \times d \tag{6}$$

2.10. Crystalline structure and water accessibility

Crystallinities and water accessibility of CNF films were analyzed by Fourier transform Raman (FT-Raman) spectroscopy on a Bruker Multi-Ram spectrometer (Bruker Instruments Inc., Billerica, MA). The crystallinity (X) was measured using 380-Raman and 93-Raman methods based on the following Eqs. (7) and (8) [20–22].

$$X_{380} = \frac{\frac{I_{380}}{I_{1096}} - 0.0286}{0.0065} \tag{7}$$

$$X_{93} = \frac{\frac{I_{93}}{I_{1096}} - 0.0182}{0.0029} \tag{8}$$

where I_{93}, I_{380}, and I_{1096} are the intensities for Raman frequencies at 93 cm^{-1}, 380 cm^{-1}, and 1096 cm^{-1} in the spectra of the samples, while X_{380} and X_{93} represent the crystallinity values estimated from bands at 380 cm^{-1} and 93 cm^{-1}.

The accessibility (A) of nanocellulose films by water at a molecular level is measured by intensity increase of the band at 1380 cm^{-1} in a CNF sample's Raman spectrum after the sample has undergone a complete OH-to-OD exchange [22–25]. Accessibility "A" is then calculated from Eq. (9):

$$A_{accessibility} = \frac{\Delta I_{sample} \times 100}{\Delta I_{amorphous}} \tag{9}$$

where I_{sample} is the relative intensity increase (%) for 1380 cm^{-1} band in the Raman spectrum of the fully OH-to-OD exchanged sample, $I_{\mathrm{amorphous}}$ is the relative intensity increase (%) for a similarly exchanged amorphous cellulose sample. $\Delta I_{\mathrm{amorphous}}$ has previously been reported to be 154.3% [22].

3. Results and discussion

3.1. Effect of mechanical fibrillation on fibril morphology

The morphology of CNFs varied with the severity of mechanical fibrillation as shown by AFM in the left panel of Fig. 1. Increasing the degree of mechanical fibrillation, i.e., increasing the number of passes in the microfluidizer, resulted in finer fibrils. The fibril height distribution quantitatively supports the visual observation from the AFM images (Fig. 1a–d). The mean CNFs height was reduced from 26 nm for P0 to 12 nm for P50. Furthermore, mechanical fibrillation also depolymerized the cellulose, the degree of polymerization (DP) of P0 was 795 and P50 was 467. DP is a measure of the length and branching of cellulose chains and can reflect the properties of CNF products [26]. Although the mean fibril height and DP decreased between P0 and P30, there was no additional change between P30 and P50.

3.2. CNF film morphology

To investigate the influence of fibril morphology on the surface of CNF films, AFM topographic and 3D images of the structure of CNF films are compared (Fig. 2). It was found that the peak-to-valley height values were 830, 470, 330 and 290 nm for the P0, P15, P30 and P50 films, respectively, from the AFM 3D images. Root mean surface (RMS)

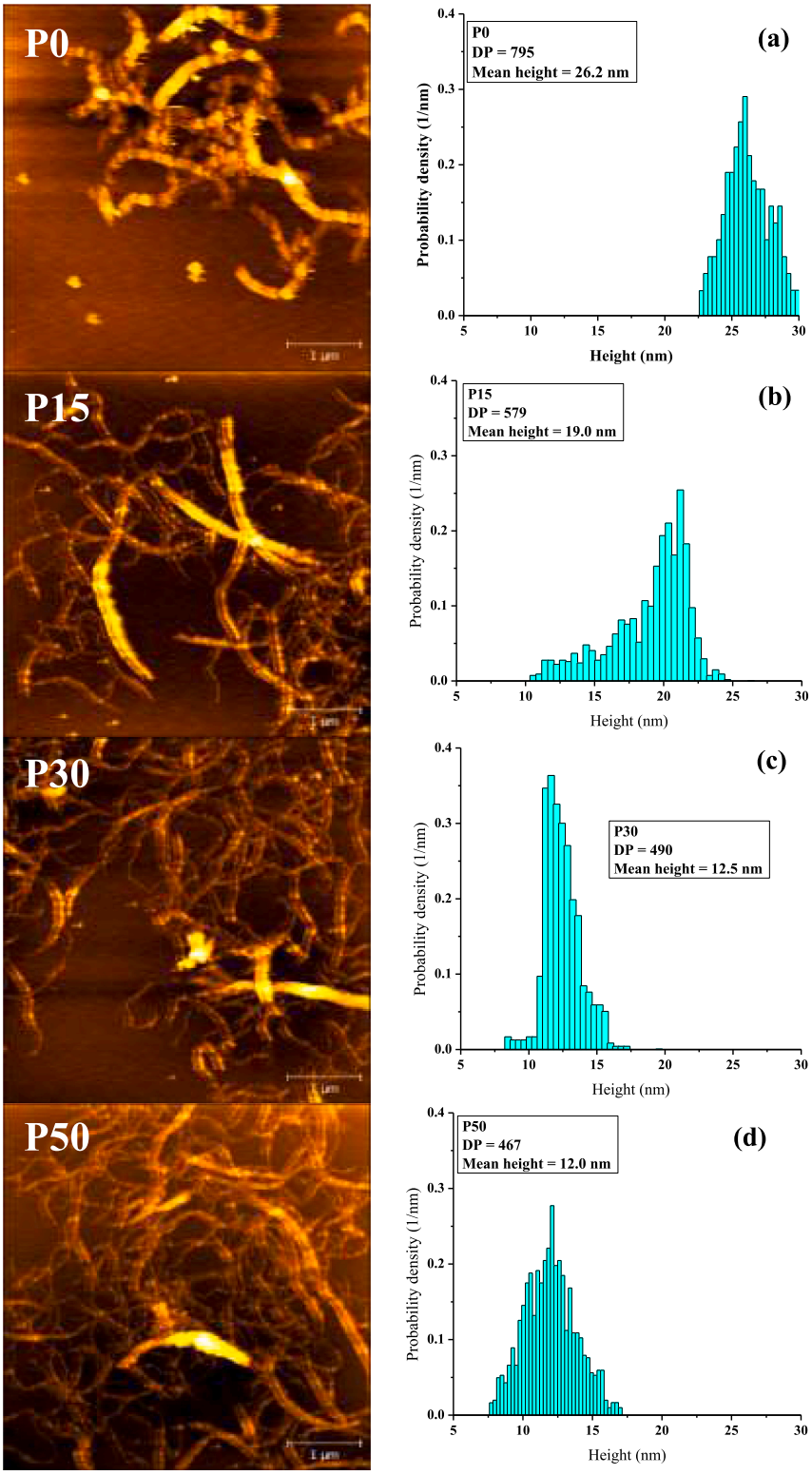

Fig. 1. Effect of the degree of mechanical fibrillation, measured by the number of passes through the microfluidizer, on the morphology of the resulting cellulose nanofibrils (CNFs) (left column) and the corresponding height distribution measured from AFM topographic data (right column) (a) 0 passes; (b) 15 passes; (c) 30 passes; and (d) 50 passes.

roughness value also can be a measure of film surface property, which is related to the diameter and distribution of fibrils. As shown in Table 1, P0 film with thicker and longer fibrils presented highest RMS roughness of 65.7 ± 0.9 nm. This may be due to the presence of numerous aggregates during film preparation. Mechanical fibrillation resulted in shorter and thinner fibrils, which produced a CNF film with an observed smoother surface and lower RMS roughness (Table 1). As with the CNF characteristics, the RMS roughness decreased between P0 and P30 but did not further decrease between P30 and P50. Although the density and porosity changed slightly between P30 and P50, additional refining

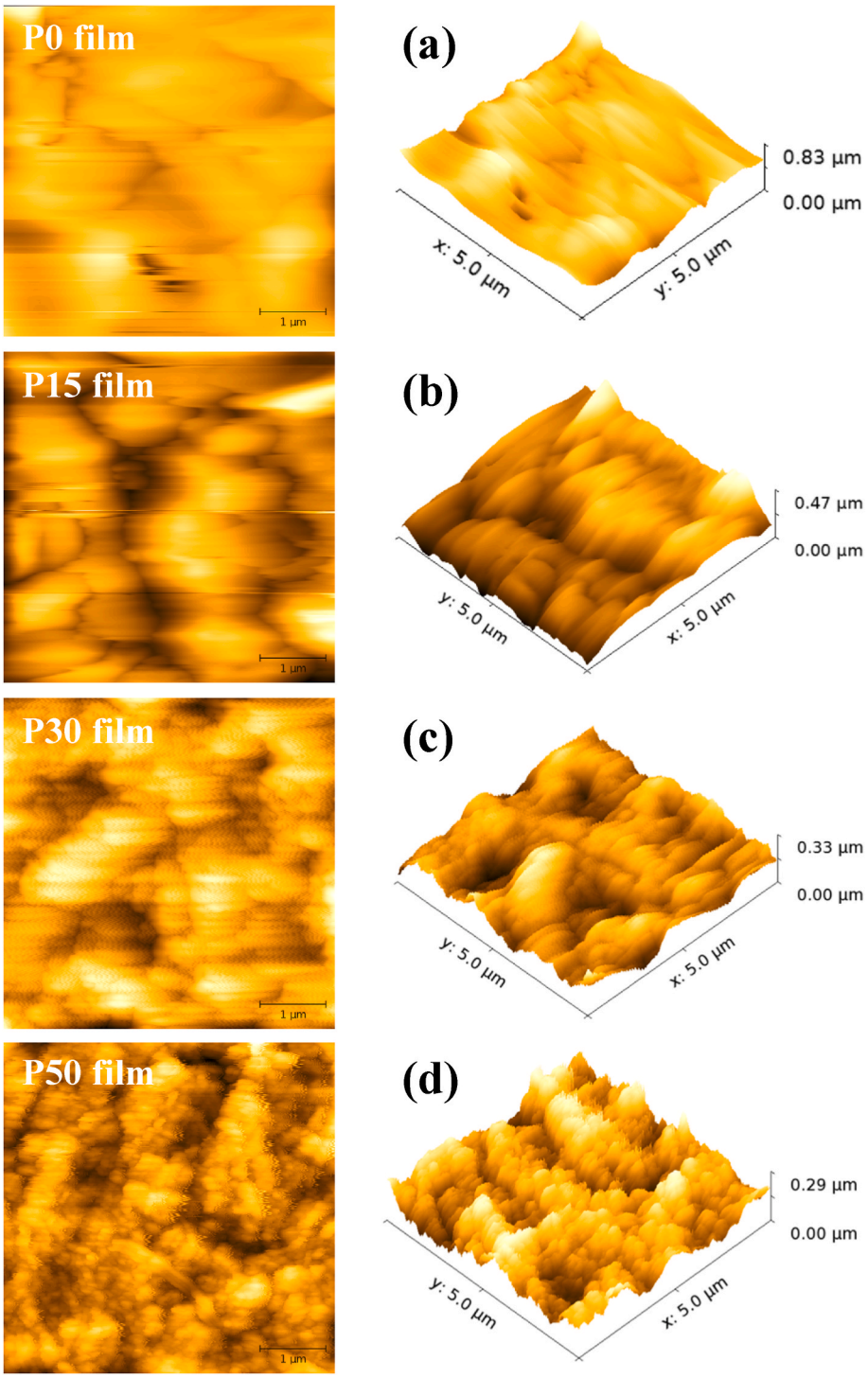

Fig. 2. AFM topographic (left panel) and 3D (right panel) images of different CNF films to describe the distribution of fibril orientation with films. Scale bar = 1μm. (a) P0 film; (b) P15 film; (c) P30 film; (d) P50 film.

Table 1
Density, porosity, Root mean surface (RMS) roughness, and mechanical properties of the CNF films. Different superscripts represent statistically significant differences.

Sample	Density (g/cm^3)	Porosity (%)	RMS roughness (nm)	Tensile strength (MPa)	Young's modulus (GPa)	Elongation at break (%)
P0	1.29 ± 0.01	14.2 ± 0.9	65.7 ± 0.9	67.0 ± 5.1^A	7.9 ± 0.4^A	5.6 ± 0.3^A
P15	1.33 ± 0.01	11.1 ± 1.0	45.6 ± 0.6	120.3 ± 11.1^B	10.5 ± 0.7^B	4.0 ± 0.4^B
P30	1.39 ± 0.01	7.1 ± 0.9	38.5 ± 3.3	164.2 ± 13.2^C	15.1 ± 1.0^C	3.6 ± 0.4^B
P50	1.44 ± 0.01	4.0 ± 0.9	36.0 ± 1.6	172.0 ± 4.6^C	11.2 ± 0.8^B	3.7 ± 0.4^B

energy beyond 30 passes provided little or no improvement in mechanical properties, suggesting that 30 passes may be the optimum processing condition.

3.3. Physical and mechanical properties

The density and porosity of different CNF films are provided in Table 1. The density of film was calculated by measuring the film weight, area and thickness using a thickness gauge meter. All of the prepared films had a density of 1.29–1.44 g/cm^3, which is consistent with the density value (0.96–1.52 g/cm^3) for the CNF films in the literature [18,26,27]. The density increased from P0 to P50 film while the porosity decreased. This suggests that shorter and thinner fibrils with higher surface area could form a stacking network in a film made of randomly arranged CNFs.

Tensile properties of the CNF films are also reported in Table 1. Tensile properties of CNF films can provide information on fiber network behavior, depending on fiber geometry, especially single fiber mechanical properties, interfiber bonding, and fiber aspect ratio. Among all the films, it can be seen the P50 film had the highest tensile strength, which was almost three times greater than the P0 films. Young's modulus, which is calculated based on the initial linear region of the strength–strain curve, strongly depends on the crystallinity of CNF. Not only did the P50 film have the highest tensile strength but it also had the highest Young's modulus value of 16.8 GPa. These results suggest that more hydrogen bonding might be formed with the increasing degrees of mechanical fibrillation, resulting in higher mechanical properties of CNF films. Strain to failure, or elongation at break, was reduced after microfluidization due to the fact that the shorter or thinner fibrils formed by mechanical fibrillation reduced the extensibility on deformation. Strain of P0 film was 5.6%, which decreased when the number of passes through microfluidizer increased.

Here, we observed that as the energy increases, the fibers become smaller, and the tensile behavior displays embrittlement in which the strength and modulus increases while the strain to break decreases. In our previous work, we found similar results and that microfluidization results in decreased DP and crystallinity of cellulose pulp fibers [28,29]. Henriksson et al. also found that CNFs prepared by enzymatic treatment and microfluidization with lower DP had higher lower strain to failures [26]. However, they also found that carboxylated CNFs had much higher mechanical properties, including toughness than those produced by enzymatic and mechanical treatments [26]. Interestingly, Zhu et al. found that more microfluidization of TEMPO-oxidized CNFs (TOCNs) led to reduced fiber diameters and increased strength and toughness of resulting papers [30]. CNFs produced without chemical pre-treatments often have much broader range of diameter distribution than TOCNs, and the resulting films also found to have higher density, likely due to better packing due to uniform fiber diameters [31]. These studies on microfluidization of CNFs indicate that the combination of chemical and mechanical treatments plays a significant impact on mechanical properties.

3.4. Optical properties

All films fabricated from CNF with or without microfluidization were visually transparent. Fig. 3 illustrates the light transmittance of films from CNFs after passing the microfluidizer for different times and digital images of the films. Transmittances follow the order of P50 > P30 > P15 > P0, indicating CNF films made of smaller fibrils have better optical transmittance. At a wavelength of 600 nm the CNF film of P0 had a white and turbid appearance with a transmittance of 37%, while the transmittance value was 65% for P50 film which is comparable with TEMPO-oxidized cellulose nanofibrils (TOCNs) film [27]. Desiccant pellets can be seen clearly through P30 and P50 films, showing the transparency of these two films, whereas desiccant pellets cannot be seen through P0 film and partially seen for P15 film.

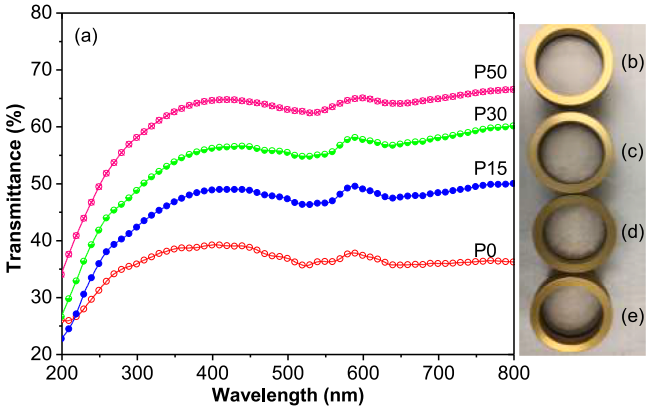

Fig. 3. Visible light transmittance of different CNF films (a) and digital image of films of P0 (b), P15 (c), P30 (d) and P50 (e) mounted over cups durinig WVP test.

3.5. Barrier properties

Good barrier properties of the crystalline regions of cellulose nanofibrils and the strong interlocking hydrogen bonds (H-bonds) within each fibril make the CNF films an excellent barrier material [32–34]. In this study both water vapor permeability (WVP) and oxygen permeability (OP) were evaluated. Water vapor permeability values for P0 to P50 films at two levels of relative humidity (RH 50% and RH 90%) are summarized in Table 2. When tested at a 50% RH, and compared with P0, the reduction of WVP significantly dropped for P30 and P50 by 41%, and 42%, respectively, suggesting that 30 passes is the optimum number of passes. When RH was increased to 90% there was no statistically significant change in WVP between P0 and films that had been microfluidized. Increases in WVP for CNF films with increase RH has been reported elsewhere, but the explanation as to why there are no differences between samples is unknown and required further investigation into the mechanism.

Oxygen permeability (OP) values for P0 to P50 films at two levels of relative humidity (RH 50% and RH 90%) are listed in Table 3. The OP for the films dramatically increased as the relative humidity increased, which is typical for CNF films [19,35]. At either 50% RH or 90% RH there was no significant difference between P0 and P50, suggesting that further microfluidization, or material density, does not significantly impact the OP of the resultant films. Also note that the coefficient of variation of OP was as much as 30% for these samples making subtle differences difficult to detect.

3.6. Crystalline structure and water accessibility

Raman spectroscopy has the capability to measure both the crystallinity and water accessibility of nanocellulose [20,23,32,36]. As processing increases the CNF crystallinity decreased and the water accessibility increased (Table 4). Before microfluidization, P0, ~34% of the cellulose is accessible to water which increases to ~42% for P50. A

Table 2
Water vapor permeability (WVP) of CNF films under two conditions.

Sample	WVP (g m)/(s m^2 Pa) (× 10^{-11})	
	RH 50%, 21.1 °C	RH 90%, 26.7 °C
P0	6.23 ± 1.52^{A}	13.7 ± 3.4^{A}
P15	5.61 ± 2.02^{A,B}	11.7 ± 1.7^{A}
P30	3.70 ± 0.80^{B,C}	10.2 ± 0.5^{A}
P50	3.62 ± 0.17^{C}	11.0 ± 1.3^{A}

Superscript letters indicate statistical significance with different letters having statistical differences at a significance level (alpha) of 0.05.

Table 3
Oxygen permeability (OP) of CNF films under two conditions.

Sample	OP (cc μm)/(m^2 day atm)	
	RH 50%, 23 °C	RH 90%, 23 °C
P0	39.8 ± 6.0^{A}	2494 ± 222^{A}
P15	28.4 ± 5.9^{B}	2610 ± 583^{A}
P30	35.0 ± 3.3^{A,B}	2205 ± 17^{A}
P50	28.1 ± 8.4^{A,B}	2139 ± 240^{A}

Superscript letters indicate statistical significance with different letters having statistical differences at a significance level (alpha) of 0.05.

Table 4
Crystallinities and water accessibilities by FT-Raman spectroscopy.

Sample	X_{380} (%)	X_{93} (%)	I_{1380} increase (%)	Water accessibility (%)
P0	47.7 ± 0.6	28.8 ± 0.8	52.2 ± 12.2	33.9 ± 7.9
P15	43.9 ± 0.3	25.6 ± 1.5	56.5 ± 7.7	36.7 ± 5.0
P30	43.6 ± 0.4	25.1 ± 1.0	57.3 ± 6.2	37.2 ± 4.1
P50	41.0 ± 0.7	22.4 ± 1.2	63.8 ± 11.8	41.5 ± 7.7

strong linear relationship exists between crystallinity and water accessibility (Fig. 4), indicating the less crystalline P50 film is more readily accessible by water.

3.7. Relationship between CNF film properties and water vapor permeability

As processing CNFs increased, the porosity of the resulting CNF films decreased, improving water vapor barrier properties. CNF films showed increasing WVP with increasing porosity when the CNF film porosity was above 7% (Fig. 5). This supports other studies demonstrating that the WVP of CNF films depends on material density [3,19,32].

In addition to film structure (density and porosity), crystallinity and water accessibility could be important factors influencing water vapor permeation of these nanocellulose films. The relationship between WVP and crystallinity is shown in Fig. 6. Interestingly, there is a positive correlation between WVP and crystallinity, indicating that the samples with higher crystallinity had poorer barrier performance. It seems likely that this is an artifact of competing phenomena. As CNFs are refined, their crystallinity decreases but their size is reduced leading to increased film density. This increased density of the films appears to be the dominant factor in controlling permeability.

The correlation between water accessibility and WVP is better at 50% RH than 90% RH but suggests that WVP decreases as water accessibility increases (Fig. 7). If water accessibility was a dominant factor in WVP, we would expect that as water accessibility increased,

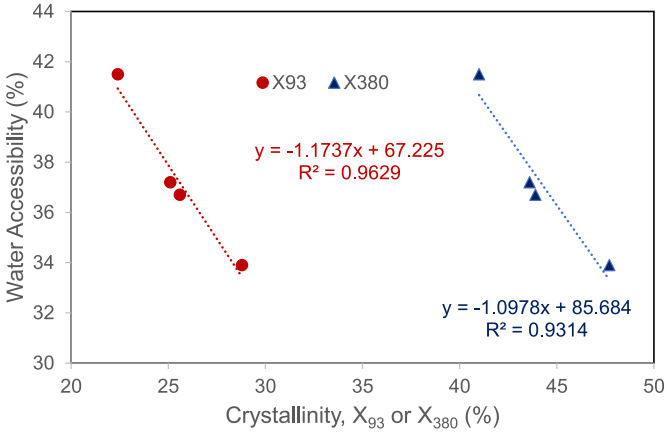

Fig. 4. Correlation between crystallinity and water accessibility of CNF films determined using FT-Raman spectroscopy.

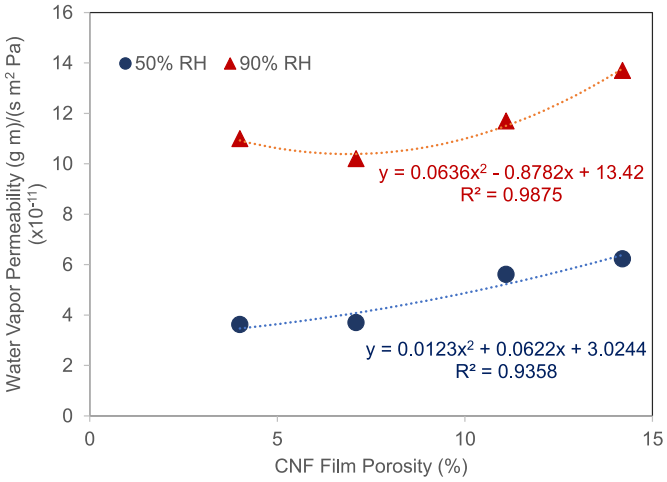

Fig. 5. Correlation between WVP and crystallinity determined using peak intensity at (a) 380 cm^{-1} and (b) 93 cm^{-1} from FT-Raman spectroscopy.

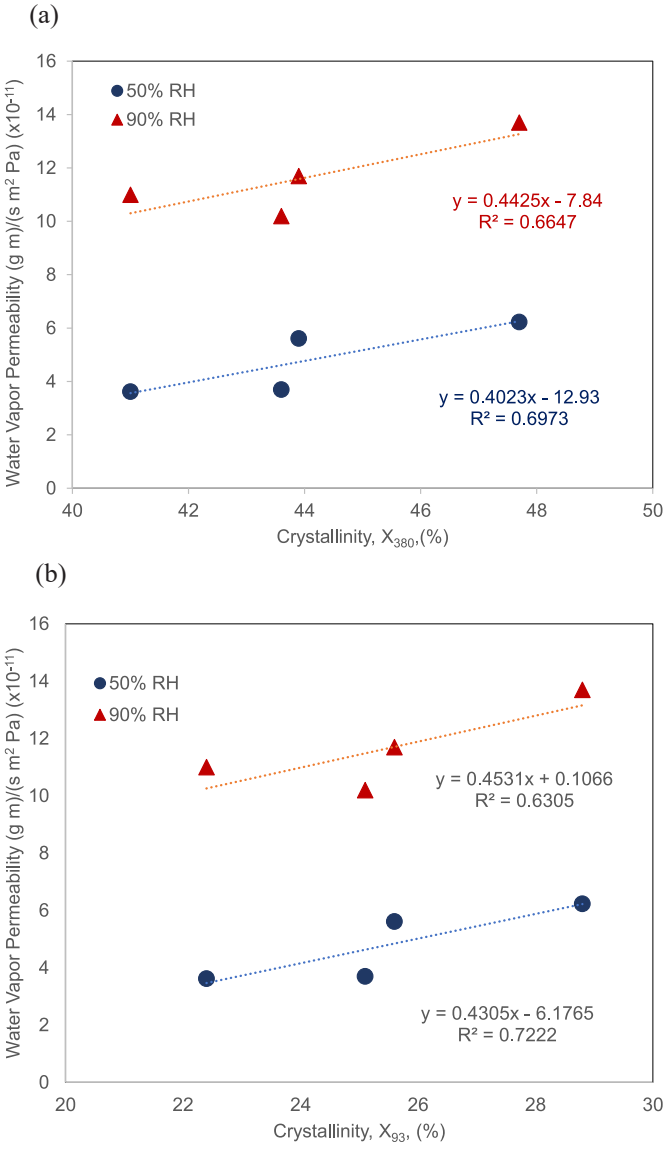

Fig. 6. Correlation between WVP and crystallinity determined using peak intensity at (a) 380 cm^{-1} and (b) 93 cm^{-1} from FT-Raman spectroscopy.

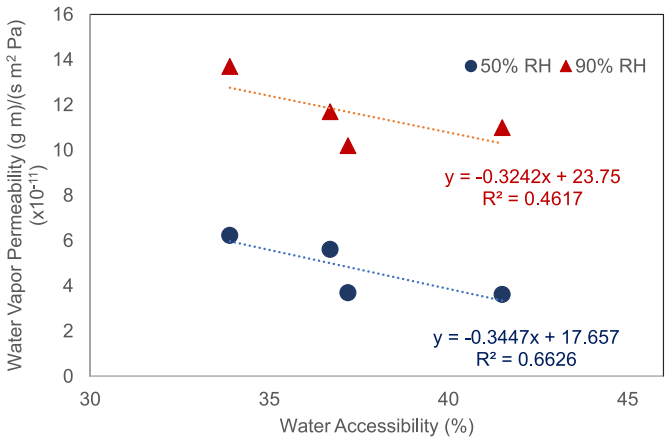

Fig. 7. Correlation between WVP and water accessibility of the CNF films.

WVP would also increase. Therefore, we suggest that the mechanism of water vapor transmission through these CNF films depends more on the physical structure of the films, i.e., porosity, rather than CNF characteristics such as crystallinity and water accessibility. More specifically, less ordered and less dense areas of the film are more accessible for water vapor permeation, while more ordered/crystalline region is less accessible for water vapor permeation. Although the most processed CNF film (e.g., P50) is more accessible by water molecules, less water molecules may be able to permeate the CNF film due to water molecules are abstracting to fibrils surfaces and hindering the path for water vapor permeation. This mechanism is shown in Fig. 8.

4. Conclusions

Cellulose nanofibrils were successfully prepared using a combination of a Super Mass Colloider followed by passes through a microfluidizer for 0 time (P0), 15 times (P15), 30 times (P30) and 50 times (P50). Significantly smaller diameter and lower degree of polymerization of CNFs were achieved when the number of passes increased from zero (P0) to 30 times (P30), and no further changes were observed between P30 and P50 samples. The surface roughness (RMS) of films decreased significantly from P0 to P50 film. P30 and P50 films showed significantly higher transparency compared to P0 and P15 films. P50 film showed the highest tensile strength and Young's modulus. Compared to P0 film, water vapor permeation was 40% and 22% lower for P30 and P50 films at 50% RH, while water vapor permeation did not significantly change at 90% RH. Oxygen permeability did not significantly change with increased processing. For P0 to P50 samples, Raman spectroscopic analysis showed crystallinity decreased while water accessibility increased. The negative correlation between water vapor permeation and water accessibility was observed because the latter depends upon the amount of non-crystalline region in CNF films, which was not the case for water vapor permeation, which seemed to be more influenced by film density than crystallinity or water accessibility. Further evaluation of the relationships between water accessibility measurements and film properties are needed to determine the utility of such measurements for evaluating cellulose-based packaging film performance. In conclusion, this study not only demonstrates the feasibility to use pure mechanical treatment to produce CNFs with good barrier properties, but also establishes the correlation between CNFs ultrastructure and performance of the resulting films. The insights gained are important for high performance packaging material applications and further investigations into the effects of these properties on barrier properties is warranted.

Funding

This research was funded by the US Endowment for Forestry and Communities, Public-Private Partnership for Nanotechnology (P3Nano). This research was supported by the US Department of Agriculture, Forest Service, Michigan State University School of Packaging, and the Jiangsu Co-Innovation Center of Efficient Processing and Utilization of Forest Resources.

Availability of data and material

The data presented in this study are available on request from the corresponding author.

Author's contributions

Conceptualization, L.W., R.S.; methodology, L.W., H.B., U.A.; R.S.; formal analysis, L.W., H.B., U.A., L.M., N.S., R.S.; investigation, L.W., H.B., U.A.; writing-original draft, L.W., U.A.; writing-review and editing, R.S., N.S., L.M.; supervision, N.S., R.S.; project administration, N.S., R.S.; funding acquisition, N.S.

Ethics approval

NA.

Consent to participate

All authors agree to participate in this research study.

Consent for publication

All authors have read and reviewed this manuscript and consent to publication.

Declaration of competing interest

The authors declare the following financial interests/personal relationships which may be considered as potential competing interests: Nicole Stark reports financial support was provided by US Endowment

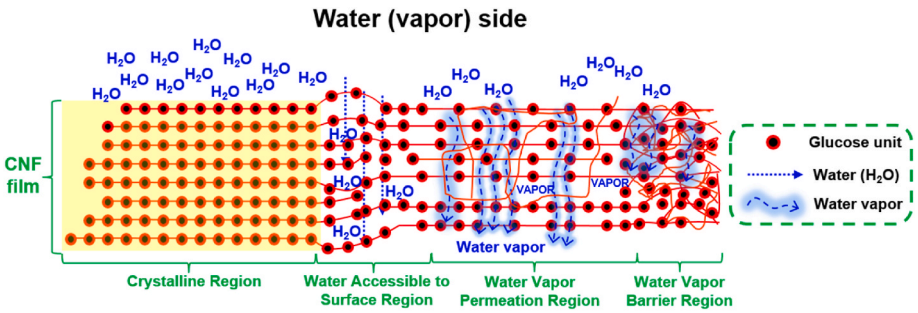

Fig. 8. Water vapor permeation and water accessibility of CNF films.

for Forestry and Communities.

Data availability

Data will be made available on request.

Acknowledgments

The authors would like to acknowledge the following people from the USDA, Forest Service, Forest Products Laboratory: Sally A. Ralph for Raman spectroscopy, Dr. J.Y. Zhu for UV–Vis spectroscopic assistance, Neil Gribbins and Philip Walsh for the help with microfluidizer, and Nancy Sutherland for assistance in tensile test.

References

[1] J. Wang, D.J. Gardner, N.M. Stark, D.W. Bousfield, M. Tajvidi, Z. Cai, Moisture and oxygen barrier properties of cellulose nanomaterial-based films, ACS Sustain. Chem. Eng. 6 (2017) 49–70, https://doi.org/10.1021/acssuschemeng.7b03523.
[2] N.M. Stark, Opportunities for cellulose nanomaterials in packaging films: a review and future trends, J. Renew. Mater. 4 (2016) 313–326, https://doi.org/10.7569/JRM.2016.634115.
[3] K.L. Spence, R.A. Venditti, O.J. Rojas, Y. Habibi, J.J. Pawlak, The effect of chemical composition on microfibrillar cellulose films from wood pulps: water interactions and physical properties for packaging applications, Cellulose 17 (2010) 835–848, https://doi.org/10.1007/s10570-010-9424-8.
[4] M. Shimizu, T. Saito, A. Isogai, Water-resistant and high oxygen-barrier nanocellulose films with interfibrillar cross-linkages formed through multivalent metal ions, J. Membr. Sci. 500 (2016) 1–7, https://doi.org/10.1016/j.memsci.2015.11.002.
[5] S. Ahankari, A. Subhedar, S. Bhadauria, A. Dufresne, Nanocellulose in food packaging: a review, Carbohydr. Polym. 255 (2021), 117479, https://doi.org/10.1016/j.carbpol.2020.117479.
[6] Q. Wang, J.Y. Zhu, Effects of mechanical fibrillation time by disk grinding on the properties of cellulose nanofibrils, Tappi J. 15 (2016) 419–423.
[7] Y. Zhao, C. Xu, C. Xing, X. Shi, L.M. Matuana, H. Zhou, X. Ma, Fabrication and characteristics of cellulose nanofibril films from coconut palm petiole prepared by different mechanical processing, Ind. Crop. Prod. 65 (2015) 96–101, https://doi.org/10.1016/j.indcrop.2014.11.057.
[8] K. Saelee, N. Yingkamhaeng, T. Nimchua, P. Sukyai, An environmentally friendly xylanase-assisted pretreatment for cellulose nanofibrils isolation from sugarcane bagasse by high-pressure homogenization, Ind. Crop. Prod. 82 (2016) 149–160, https://doi.org/10.1016/j.indcrop.2015.11.064.
[9] M. Pääkkö, M. Ankerfors, H. Kosonen, A. Nykänen, S. Ahola, M. Österberg, J. Ruokolainen, J. Laine, P.T. Larsson, O. Ikkala, T. Lindström, Enzymatic hydrolysis combined with mechanical shearing and high-pressure homogenization for nanoscale cellulose fibrils and strong gels, Biomacromolecules 8 (2007) 1934–1941, https://doi.org/10.1021/bm061215p.
[10] S. Iwamoto, A.N. Nakagaito, H. Yano, Nano-fibrillation of pulp fibers for the processing of transparent nanocomposites, Appl. Phys. A 89 (2007) 461–466, https://doi.org/10.1007/s00339-007-4175-6.
[11] I.S. Sacui, R.C. Nieuwendaal, D.J. Burnett, S.J. Stranick, M. Jorfi, C. Weder, E. J. Foster, R.T. Olsson, J.W. Gilman, Comparison of the properties of cellulose nanocrystals and cellulose nanofibrils isolated from bacteria, tunicate, and wood processed using acid, enzymatic, mechanical, and oxidative methods, ACS Appl. Mater. Interfaces 6 (2014) 6127–6138, https://doi.org/10.1021/am500359f.
[12] H. Bian, Y. Gao, Y. Yang, G. Fang, H. Dai, Improving cellulose nanofibrillation of waste wheat straw using the combined methods of prewashing, p-toluenesulfonic acid hydrolysis, disk grinding, and endoglucanase post-treatment, Bioresour. Technol. 256 (2018) 321–327, https://doi.org/10.1016/j.biortech.2018.02.038.
[13] S.S. Nair, J.Y. Zhu, Y. Deng, A.J. Ragauskas, Characterization of cellulose nanofibrillation by micro grinding, J. Nanoparticle Res. 16 (2014) 2349–2359, https://doi.org/10.1007/s11051-014-2349-7.
[14] Q.Q. Wang, J.Y. Zhu, R. Gleisner, T.A. Kuster, U. Baxa, S.E. McNeil, Morphological development of cellulose fibrils of a bleached eucalyptus pulp by mechanical fibrillation, Cellulose 19 (2012) 1631–1643, https://doi.org/10.1007/s10570-012-9745-x.
[15] Y.L. Qin, X. Qiu, J.Y. Zhu, Understanding longitudinal wood fiber ultra-structure for producing cellulose nanofibrils using disk milling with diluted acid prehydrolysis, Sci. Rep. 6 (2016), 35602, https://doi.org/10.1038/srep35602.
[16] U.P. Agarwal, Raman spectroscopy in the analysis of cellulose nanomaterials, in: U. P. Agarwal, R.H. Atalla, A. Isogai (Eds.), Nanocelluloses: Their Preparation, Properties, and Applications, ACS Publications, 2017, https://doi.org/10.1021/bk-2017-1251.
[17] R.W. Reiner, A.W. Rudie, Pilot plant scaleup of TEMPO-pretreaded cellulose nanofibrils, in: M.T. Postek, R.J. Moon, A.W. Rudie, M.A. Bilodeau (Eds.), Production and Applications of Cellulose Nanomaterials, 2013, 978-1-59510-224-9.
[18] Y. Qing, R. Sabo, J.Y. Zhu, U. Agarwal, Z. Cai, Y. Wu, A comparative study of cellulose nanofibrils disintegrated via multiple processing approaches, Carbohydr. Polym. 97 (2013) 226–234.
[19] R. Wang, L. Chen, J.Y. Zhu, R. Yang, Tailored and integrated production of carboxylated cellulose nanocrystals (CNC) with nanofibrils (CNF) through maleic acid hydrolysis, ChemNanoMat 3 (2017) 328–335, https://doi.org/10.1002/cnma.201700015.
[20] U.P. Agarwal, R.S. Reiner, S.A. Ralph, Cellulose I crystallinity determination using FT–Raman spectroscopy: univariate and multivariate methods, Cellulose 17 (2010) 721–733, https://doi.org/10.1007/s10570-010-9420-z.
[21] U.P. Agarwal, S.A. Ralph, R.S. Reiner, Estimation of cellulose crystallinity of lignocelluloses using near-IR FT-Raman spectroscopy and comparison of the Raman and segal-WAXS methods, J. Agric. Food Chem. 61 (2013) 103–113, https://doi.org/10.1021/jf304465k.
[22] U.P. Agarwal, S.A. Ralph, R.S. Reiner, C. Baez, Probing crystallinity of never-dried wood cellulose with Raman spectroscopy, Cellulose 23 (2016) 125–144, https://doi.org/10.1007/s10570-015-0788-7.
[23] U.P. Agarwal, S.A. Ralph, R.S. Reiner, C. Baez, New cellulose crystallinity estimation method that differentiates between organized and crystalline phases, Carbohydr. Polym. 190 (2018) 262–270, https://doi.org/10.1016/jcarbpol.2018.003.
[24] U.P. Agarwal, S.A. Ralph, R.S. Reiner, C. Baez, Probing crystallinity of never-dried wood cellulose with Raman spectroscopy, Cellulose 23 (2015) 125–144, https://doi.org/10.1007/s10570-015-0788-7.
[25] U.P. Agarwal, Raman spectroscopy in the analysis of cellulose nanomaterials, in: Nanocelluloses: Their Preparation, Properties, and Applications, ACS Publications, 2017, pp. 75–90.
[26] M. Henriksson, L.A. Berglund, P. Isaksson, T. Lindström, T. Nishino, Cellulose nanopaper structures of high toughness, Biomacromolecules 9 (2008) 1579–1585, https://doi.org/10.1021/bm800038n.
[27] Z. Fang, H. Zhu, Y. Yuan, D. Ha, S. Zhu, C. Preston, Q. Chen, Y. Li, X. Han, S. Lee, G. Chen, T. Li, J. Munday, J. Huang, L. Hu, Novel nanostructured paper with ultrahigh transparency and ultrahigh haze for solar cells, Nano Lett. 14 (2014) 765–773, https://doi.org/10.1021/nl404101p.
[28] Y. Qing, R. Sabo, J.Y. Zhu, Z. Cai, Y. Wu, Comparative study of cellulose nanofibrils disintegrated from different approaches, in: Advancements in Fiber-Polymer Composites: Wood Fiber, Natural Fibers, and Nanocellulose, Milwaukee, WI, 2013.
[29] Y. Qing, R. Sabo, J.Y. Zhu, U. Agarwal, Z. Cai, Y. Wu, A comparative study of cellulose nanofibrils disintegrated via multiple processing approaches, Carbohydr. Polym. 97 (2013) 226–234, https://doi.org/10.1016/j.carbpol.2013.04.086.
[30] H. Zhu, S. Zhu, Z. Jia, S. Parvinian, Y. Li, O. Vaaland, L. Hu, T. Li, Anomalous scaling law of strength and toughness of cellulose nanopaper, Proc. Natl. Acad. Sci. USA 112 (29) (2015) 8971–8976.
[31] Y. Qing, R. Sabo, Y. Wu, J.Y. Zhu, Z. Cai, Self-assembled optically transparent cellulose nanofibril films: effect of nanofibril morphology and drying procedure, Cellulose 22 (2015) 1091–1102.
[32] E. Rojo, M.S. Peresin, W.W. Sampson, I.C. Hoeger, J. Vartiainen, J. Laine, O. J. Rojas, Comprehensive elucidation of the effect of residual lignin on the physical, barrier, mechanical and surface properties of nanocellulose films, Green Chem. 17 (2015) 1853–1866, https://doi.org/10.1039/C4GC02398F.
[33] A. Ferre, I. Quintana Ec Filpponen, I. Solala, T. Vidal, A. Rodríguez, J. Laine, O. J. Rojas, Effect of residual lignin and heteropolysaccharides in nanofibrillar cellulose and nanopaper from wood fibers, Cellulose 19 (2012) 2179–2193, https://doi.org/10.1007/s10570-012-9788-z.
[34] R.T. Olsson, M.A.S. Azizi Samir, G. Salazar-Alvarez, L. Belova, V. Ström, L. A. Berglund, O. Ikkala, J. Nogués, U.W. Gedde, Making flexible magnetic aerogels and stiff magnetic nanopaper using cellulose nanofibrils as templates, Nat. Nanotechnol. 5 (2010) 584–588, https://doi.org/10.1038/nnano.2010.1.
[35] R.A. Lafia-Araga, R. Sabo, O. Nabinejad, L. Matuana, N. Stark, Influence of lactic acid surface modification of cellulose nanofibrils on the properties of cellulose nanofibril films and cellulose nanofibril-poly(lactic acid) composites, Biomolecules 11 (2021) 1346, https://doi.org/10.3390/biom11091346.
[36] E.J. Foster, R.J. Moon, U.P. Agarwal, M.J. Bortner, J. Bras, S. Camarero-Espisosa, K.J. Chan, M.J.D. Clift, E.D. Cranston, S.J. Eichorn, D.M. Fox, W.Y. Hamad, L. Heux, B. Jean, M. Korey, W. Neih, K.J. Ong, M.S. Reid, S. Renneckar, R. Roberty, J. Shatkin, J. Simonsen, K. Stinson-Bagby, N. Wanasekara, J. Youngblood, Current characterization methods for cellulose nanomaterials, Chem. Soc. Rev. 47 (2018) 2609–2679, https://doi.org/10.1039/C6CS00895J.